Available online at www.sciencedirect.com
ScienceDirect
Journal of Sound and Vibration 319 (2009) 753–767
JOURNAL OF SOUND AND VIBRATION
www.elsevier.com/locate/jsvi

Human simulated intelligent control of vehicle suspension system with MR dampers

Miao Yu[a,*], X.M. Dong[a], S.B. Choi[b], C.R. Liao[a]

[a]*Key Lab of Optoelectronic Technology and System, Education Ministry, Department of Optoelectronic Engineering, Chongqing University, 400044 Chongqing, China*
[b]*Department of Mechanical Engineering, Smart Structures and Systems Laboratory, Inha University, Incheon 402-751, Republic of Korea*

Received 16 September 2007; received in revised form 19 April 2008; accepted 21 June 2008
Handling Editor: J. Lam
Available online 13 August 2008

Abstract

This paper presents vibration control responses of a controllable magnetorheological (MR) suspension system of a passenger car. The MR damper is designed and manufactured on the basis of the mixed-mode operation, and its time response is experimentally evaluated to integrate with the suspension model. After formulating the dynamic model of a half-car MR suspension system, a human simulated intelligent control (HSIC) scheme is developed to attenuate unwanted vibrations such as pitch angle acceleration. After verifying the effectiveness of the HSIC via computer simulation, the road test of the passenger car installed with four MR dampers is undertaken. The power spectrum densities of dynamic motions such as body acceleration and pitch angle acceleration are measured and analyzed. In addition, the control results obtained from the proposed HSIC are compared with those obtained from a conventional linear quadratic Gaussian (LQG) control method.

1. Introduction

Recently, the research on the vibration suppression of a vehicle system using the semi-active suspension has been significantly increased. Though the passive suspension system featuring conventional oil or gas damper provides design simplicity and cost effectiveness, performance limitations are inevitable due to the uncontrollable damping force. On the other hand, the active suspension system can provide high control performance in wide frequency range. However, the active suspension requires high power consumption, many sensors, servo-valves, and sophisticated control logics. Consequently, the effective way to resolve these problems is to adopt the semi-active suspension system. The semi-active suspension system offers a desirable performance generally enhanced in the active mode without requiring large power consumption and expensive hardware. For the last decade, a very attractive semi-active suspension system featuring an electrorheological

*Corresponding author. Tel.: +86 023 65111016; fax: +86 023 65103126.
E-mail addresses: yumiao@cqu.edu.cn (M. Yu), seungbok@inha.ac.kr (S.B. Choi).

0022-460X/$ - see front matter © 2008 Elsevier Ltd. All rights reserved.
doi:10.1016/j.jsv.2008.06.047

(ER) fluid or magnetorheological (MR) fluid has been proposed by many investigators. Especially, the semi-active suspension system featuring MR damper has been successfully implemented in practice [1].

MR fluids are materials that respond to an applied magnetic field with a change in rheological behavior such as yield stress. Therefore, using the controllable MR fluid it is very easy to fabricate effective actuators for vibration or position control systems. Carlson et al. [2] proposed a commercially available MR damper which is applicable to on-and-off-highway vehicle suspension systems. They experimentally demonstrated that sufficient levels of damping force and also superior control capability of the damping force by applying a control magnetic field could be achieved. A dynamic model for prediction of damping force of MR damper was proposed by Spencer Jr. et al. [3]. Wereley and Pang [4] developed nonlinear quasi-steady ER and MR damper models using an idealized Bingham plastic shear flow mechanism. Dogruer and Gordaninejad et al. [5] developed a controllable, semi-active MR damper for a high mobile multipurpose wheeled vehicle. A passenger vehicle suspension system, equipped with MR dampers and H_∞ control scheme, has been developed by Choi et al. [6]. Bodie and Hac [7] used continuously variable MR dampers to distribute the damping forces between front and rear axles in order to bring the vehicle yaw rate as close as possible to the desired yaw rate. Hagiwara et al. [8] presented a design method of a smart control semi-active suspension system with a reduced number of sensors used for a full-car model. Petek et al. [9] constructed a semi-active full suspension system consisting of four ER dampers and evaluated its effectiveness for vibration isolation. They demonstrated experimentally that unwanted pitch, heave and roll motions of the vehicle body were favorably suppressed using the simple skyhook control algorithm. Liu et al. [10] proposed a fuzzy sliding mode control for a real vehicle. Experiment results show the effectiveness of this new algorithm. Koo et al. [11] studied the response time of a commercially available MR fluid damper at low piston velocities from 2.54 to 76.2 mm/s. Measured results indicate that system compliance has a significant effect on the response time of the damper.

Despite many research works on the semi-active MR suspension system, the research work on the design of a sophisticated control scheme considering time delay of the MR damper is very rare. Moreover, the investigation of control performance of the vehicle equipped with MR suspension through road test is very few. Consequently, the main contribution of this work is to design an effective control scheme for MR suspension system and verify superior control performance via road test. In order to achieve this goal, a cylindrical MR damper is designed and manufactured on the basis of the mixed-mode operation, and its time response is experimentally evaluated. After formulating the dynamic model of a half-car MR suspension system, a human simulated intelligent control (HSIC) scheme is developed to attenuate unwanted vibrations such as acceleration. After verifying the effectiveness of the HSIC via computer simulation, the road test of the passenger car installed with four MR dampers is undertaken. Control responses such as body acceleration and pitch angle acceleration are evaluated and compared with those obtained from conventional linear quadratic Gaussian (LQG) control method.

2. MR damper

Most devices that use controllable fluids can be classified as having either fixed poles (valve mode) or relatively moveable poles (direct-shear mode) [12]. For the automotive application, the MR dampers designed in this paper work as mixed-mode operation of valve mode and direct-shear mode. Fig. 1 presents its configuration. This MR damper has a twin-tube structure, which can operate with flow and shear modes. The MR damper is divided into the left and right chamber by the piston, and it is fully filled with the MR fluid. During the piston motion from the left to the right, the MR fluid flows through the gap between the inner cylinder and the piston. The magnetic field exists in the gap perpendicular to the motion direction of the MR fluid after the current is applied to the coil. The viscosity of the MR fluid in the gap is changed subjected to the magnet field and the pressure drop across the piston varies. Thus, the damping force of the MR damper is controllable by the intensity of the magnetic field. The diameter of the outer and inner cylinder is 50 and 48 mm, respectively. The compressed length of the MR damper is 330 mm. When it is extended, it reaches 508 mm. The dimensions of the MR damper have been determined by considering the geometry of the test car. Fig. 2 shows the photograph of the MR damper manufactured in this work.

In order to investigate the dynamic bandwidth of the MR damper, the damping forces to the step input are measured. Fig. 3 presents the schematic configuration of the test apparatus for the measurement of time

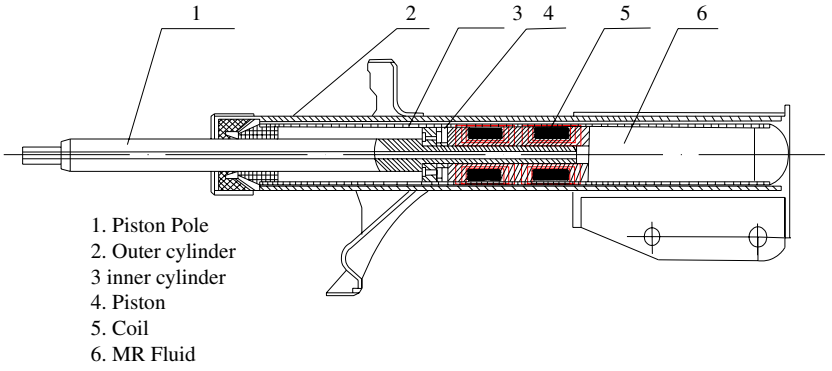

Fig. 1. Schematic configuration of the proposed mixed-mode MR damper.

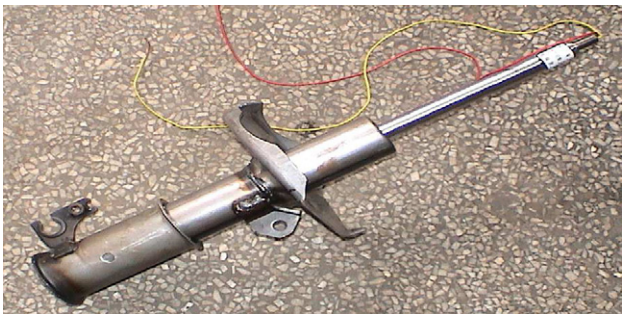

Fig. 2. Photograph of the manufactured MR damper.

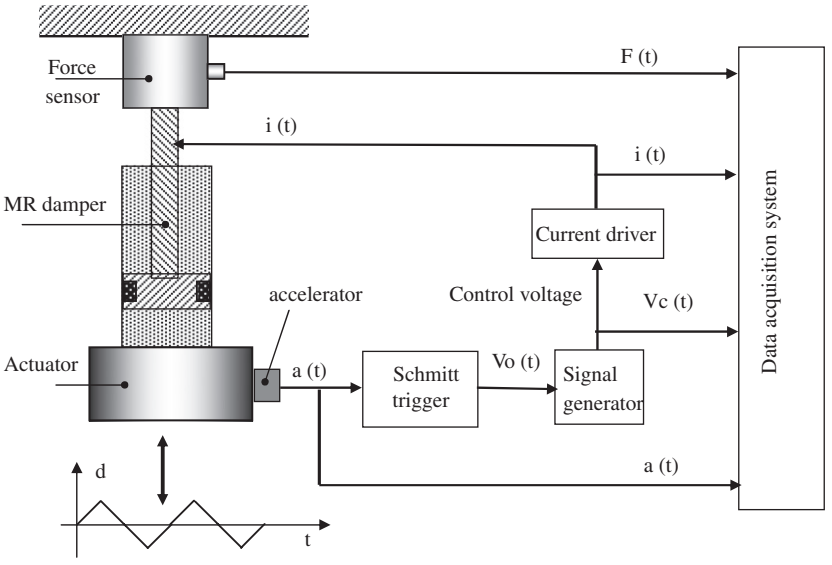

Fig. 3. Experimental apparatus for the response time and damping force measurement.

response and damping force of the MR damper. The MR damper is actuated by material test system (MTS) load frame. The damper is mounted in the load frame of the MTS. Because we are only concerned with the change in force due to the control input, the force change due to the velocity complicates the analysis. This peak signal could be transformed into passive pulse $V_0(t)$ by a Schmitt trigger. The pulse signal was then used to trigger the signal generator to get a continuous square wave $V_c(t)$ applied to the current driver as a step

control signal. So the current driver would generate various current levels from 0 to 2.5 A to adjust the damping force $F(t)$ of the MR damper. A piezoelectric force sensor was used to measure the dynamic response of MR damper. All of the signals were recorded by data acquisition system. It is noted that the trigger signal is important to ensure that the dynamic response process of the MR damper would begin at the same phase per period. Fig. 4 presents the measured step response of the MR damper. The time constant is defined as the time to reach from the initial state to the 63.2% of the final state. The time responses are investigated by changing the input current level at fixed piston velocity and also by changing the piston velocity at fixed input current. The evaluated time constant are presented in Tables 1 and 2. It is seen from Table 1 that the response time is not affected by the current level in both rising and falling cases. It is also observed that the response time in the falling case is slower than the rising case. This may be due to the effect of remanence in coils. However, this effect can be demagnetized by applying countercurrent to the coils to reduce the response time. Therefore, in this work, the response time in the rising case is only considered in the model. On the other hand, the response

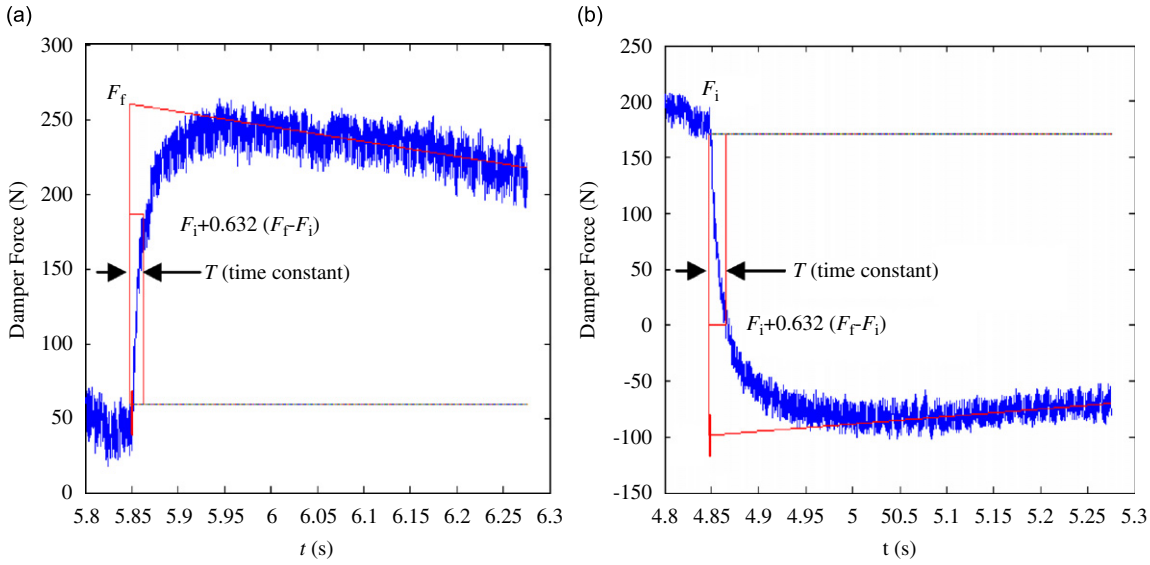

Fig. 4. Time response of the damping force under step current input. (a) Response of step-up input, (b) response of step-down input.

Table 1
Response time of MR damper at various current levels (0.1 m/s)

τ (ms)	I (A)						
	0.8	1.0	1.2	1.4	1.6	1.8	2.0
Response times in rising	14.1	14.3	14.9	14.8	16.6	14.7	13.9
Response times in falling	16.0	17.8	17.8	18.7	18.4	18.8	19.0

Table 2
Response time of MR damper at various piston velocities (1.5 A)

τ (ms)	V (m/s)					
	0.05	0.1	0.15	0.2	0.25	0.3
Response times in rising	12.4	15.5	19.2	23.3	24.5	26.1
Response times in falling	30.1	32.0	34.3	35.5	36.7	39.1

time is very sensitive to the piston velocity as shown in Table 2. Thus, the time constant of the proposed MR damper can be modeled as follows:

$$\tau = 56.914V + 10.207 \tag{1}$$

In the above, τ is the time constant and V the piston velocity. This model will be incorporated into the dynamic model of the vehicle suspension system.

This time delay is due to a combination of power supply dynamics, magnetic circuit dynamics, fluid rheology effects, and fluid compressibility effects. However, it is difficult to measure the relation MR's time delay and fluid rheology effects or fluid compressibility effects. The MR's time delay considering the effects of fluid rheology effects or fluid compressibility effects can be only calculated. Therefore, we measure the MR's time delay with different velocities and input currents. Although the MR's time delay is a variable, the velocity of MR's piston located mainly near 0.1 m/s, and the control current is limited no more than 1.5 A, the time delay of MR damper can be looked as a constant. In this paper, it is dealt with 23 ms.

3. Suspension model

In order to develop an effective control scheme, a half-car MR suspension dynamic model shown in Fig. 5 is formulated. By considering vertical and pitch motions, the governing equation of the suspension model is derived as follows:

$$\begin{aligned} m_s\ddot{Z}_s = & -(C_{sf}+C_{sr})\dot{z}_s + (C_{sf}a - C_{sr}b)\dot{\theta} - K_{sf}(z_{sf}-z_{uf}) + C_{sf}\dot{z}_{uf} \\ & - K_{sr}(z_{sr}-z_{ur}) + C_{sr}\dot{z}_{ur} + F_{fMR} + F_{rMR} \end{aligned} \tag{2}$$

$$\begin{aligned} I_y\ddot{\theta} = & (aC_{sf} - bC_{sr})\dot{z} - (C_{sf}a^2 + C_{sr}b^2)\dot{\theta} + aK_{sf}(z_{sf}-z_{uf}) - aC_{sf}\dot{z}_{uf} \\ & - bK_{sr}(z_{sr}-z_{ur}) - bC_{sr}\dot{z}_{ur} - aF_{fMR} + bF_{rMR} \end{aligned} \tag{3}$$

$$m_{uf}\ddot{z}_{uf} = C_{sf}\dot{z} - aC_{sf}\dot{\theta} + K_{sf}(z_{sf}-z_{uf}) - C_{sf}\dot{z}_{uf} - K_{tf}(Z_{uf}-Z_{rf}) - F_{fMR} \tag{4}$$

$$m_{ur}\ddot{z}_{ur} = C_{sr}\dot{z} + bC_{sr}\dot{\theta} + K_{sr}(z_{sr}-z_{ur}) - C_{sr}\dot{z}_{ur} - K_{tr}(Z_{ur}-Z_{rr}) - F_{rMR} \tag{5}$$

where z_{sf} is the fore-suspension sprung mass displacement given by $z_{sf} = z_s - a\sin\theta \approx z_s - a\theta$ and z_{sr} is the rear-suspension sprung mass displacement given by $z_{sr} = z + b\sin\theta \approx z + b\theta$. The governing equation is rewritten in the state space representation by adopting the following state variables:

$$x = [x_1x_2x_3x_4x_5x_6x_7x_8x_9x_{10}]^T = [z_s\dot{z}_s\theta\dot{\theta}z_{sf} - z_{uf}\dot{z}_{uf}z_{sr} - z_{ur}\dot{z}_{ur}z_{uf} - z_{rf}z_{ur} - z_{rr}]^T$$

where x_1 is the displacement of the suspension, x_2 the absolute velocity of the sprung mass, x_3 the pitch angle of the suspension, x_4 the pitch angle velocity, x_5 the relative displacement of the fore-suspension, x_6 the absolute velocity of the fore-sprung mass, x_7 the relative displacement of the rear-suspension, x_8 the absolute velocity of the rear-sprung mass, x_9 the fore-tire deflection, and x_{10} the rear-tire deflection. Now, by

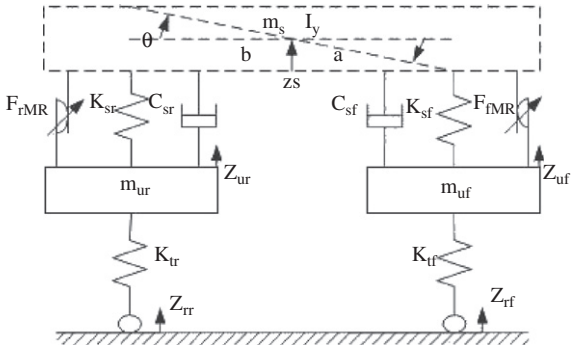

Fig. 5. Half-vehicle model.

integrating the time constant of the MR damper given in Eq. (1) with the governing equations, the state space model can be expressed as follows:

$$\dot{x} = Ax + Bu(t-\tau) + L\dot{w} \tag{6}$$

$$y = Cx \tag{7}$$

$$u(t-\tau) = [F_{\mathrm{fMR}}(t-\tau), F_{\mathrm{rMR}}(t-\tau)]^{\mathrm{T}} = -Gy(t-\tau) \tag{8}$$

In the above equation, w is the white noise input [20], G the feedback gain matrix, and C the output matrix. And the system matrix A, input matrix B, and excitation matrix L are given as follows:

$$A = \begin{pmatrix}
0 & 1 & 0 & 0 & 0 & 0 & 0 & 0 & 0 & 0 \\
0 & \frac{-(C_{\mathrm{sf}}+C_{\mathrm{sr}})}{m_s} & 0 & \frac{(aC_{\mathrm{sf}}-bC_{\mathrm{sr}})}{m_s} & \frac{-K_{\mathrm{sf}}}{m_s} & \frac{C_f}{m_s} & \frac{-K_{\mathrm{sr}}}{m_s} & \frac{C_{\mathrm{sr}}}{m_s} & 0 & 0 \\
0 & 0 & 0 & 1 & 0 & 0 & 0 & 0 & 0 & 0 \\
0 & \frac{(aC_{\mathrm{sf}}-bC_{\mathrm{sr}})}{I_y} & 0 & \frac{-(a^2C_{\mathrm{sf}}+b^2C_{\mathrm{sr}})}{I_y} & \frac{aK_{\mathrm{sf}}}{I_y} & \frac{-aC_{\mathrm{sf}}}{I_y} & \frac{-bK_{\mathrm{sr}}}{I_y} & \frac{-bC_{\mathrm{sr}}}{I_y} & 0 & 0 \\
0 & 1 & 0 & -a & 0 & -1 & 0 & 0 & 0 & 0 \\
0 & \frac{C_{\mathrm{sf}}}{m_{\mathrm{uf}}} & 0 & \frac{-aC_{\mathrm{sf}}}{m_{\mathrm{uf}}} & \frac{K_{\mathrm{sf}}}{m_{\mathrm{uf}}} & \frac{-C_{\mathrm{sf}}}{m_{\mathrm{uf}}} & 0 & 0 & \frac{-K_{\mathrm{tf}}}{m_{\mathrm{uf}}} & 0 \\
0 & 1 & 0 & b & 0 & 0 & 0 & -1 & 0 & 0 \\
0 & \frac{C_{\mathrm{sr}}}{m_{\mathrm{ur}}} & 0 & \frac{bC_{\mathrm{sr}}}{m_{\mathrm{ur}}} & 0 & 0 & \frac{K_{\mathrm{sr}}}{m_{\mathrm{ur}}} & \frac{-C_{\mathrm{sr}}}{m_{\mathrm{ur}}} & 0 & \frac{-K_{\mathrm{tr}}}{m_{\mathrm{ur}}} \\
0 & 0 & 0 & 0 & 0 & 1 & 0 & 0 & 0 & 0 \\
0 & 0 & 0 & 0 & 0 & 0 & 0 & 1 & 0 & 0
\end{pmatrix}$$

$$B = \begin{pmatrix}
0 & 0 \\
\frac{1}{m_s} & \frac{1}{m_s} \\
0 & 0 \\
\frac{-a}{I_y} & \frac{b}{I_y} \\
0 & 0 \\
\frac{-1}{m_{\mathrm{uf}}} & 0 \\
0 & 0 \\
0 & \frac{-1}{m_{\mathrm{ur}}} \\
0 & 0 \\
0 & 0
\end{pmatrix} \qquad L = \begin{pmatrix}
0 & 0 \\
0 & 0 \\
0 & 0 \\
0 & 0 \\
0 & 0 \\
0 & 0 \\
0 & 0 \\
0 & 0 \\
0 & -1 \\
-1 & 0
\end{pmatrix}$$

4. Controller design

In this work, an HSIC scheme which is one of intelligent control theories [12,13,14] is formulated and implemented for vibration control of the proposed MR suspension system. The HSIC was firstly proposed by Prof. Zhou [15] in 1979, and was published in 1983. After 24 years, the HSIC theory has been developed as an

integrity theory, which has been successfully applied in many perplexing processes and plants (such as delay system, multivariable system, nonlinear system, etc.). With HSIC method, Li et al. [13] have solved the swinging-up control of the single pendulum under limited torque. The HSIC is a multilevel hierarchical structure information processing system with three levels including direct control level, parameter correction level and task adjustment level. In this paper, the first level is to decide an appropriate based on characteristic mode of the vehicle suspension. The potential control schemes for MR damper include bang–bang control, holding mode control, proportional plus differential control and positive feedback restraining control. The second level is parameter correction level in which the system and control parameters are adaptively adjusted. The third level is task adjustment level in which both the linearization of the nonlinear MR damper and time-delay compensation for control system are considered.

4.1. Direct control level

The real line trace shown in Fig. 6 is the ideal target trajectory $f_d(e,\dot{e})$. In this equation, e represents the $\dot{z}_{sf}$ or $\dot{z}_{sr}$ and $\dot{e}$ denotes the $\ddot{z}_{sf}$ or $\ddot{z}_{sr}$. In the figure, δ_1 and δ_2 are threshold values of error and derivation of error, therefore, the figure can be called as ideal time phase plot. The red line represents the ideal dynamic trajectory of semi-active system with regulation of controller. Φ_{11}–Φ_{15} denote the different region of time phase plot, corresponding to those regions, the control gains can be determined by simulation of expert's experiences. For example, control gains keep invariant in Φ_{11} for that the states of system are located near equilibrium position. The following methods are taken to keep actual error trajectory close to the ideal error trajectory.

A characteristic element set is chosen as follows:

$$Q_1 = \{q_{11}, q_{12}, q_{13}, q_{14}, q_{15}\} \tag{9}$$

in which $q_{11} \Rightarrow |e| < \delta_1$, $q_{12} \Rightarrow |\dot{e}| < \delta_2$, $q_{13} \Rightarrow e\dot{e} > 0$, $q_{14} \Rightarrow |\dot{e}/e| < c_1$, $q_{15} \Rightarrow |\dot{e}/e| < c_2$, and c_1, c_2 are the slopes of line S_1 and S_2.

Characteristic model can be written as

$$\Phi_1 = \{\phi_{11}, \phi_{12}, \phi_{13}, \phi_{14}, \phi_{15}\} \tag{10}$$

In the above equation, $\phi_{11} = (\bar{q}_{11} \cup \bar{q}_{12}) \cap q_{13})$, $\phi_{13} = (\bar{q}_{11} \cup \bar{q}_{12}) \cap \bar{q}_{14} \cap q_{15}$, $\phi_{14} = (\bar{q}_{11} \cup \bar{q}_{12}) \cap \bar{q}_{13} \cap \bar{q}_{15}$.

The control mode set of the direct control level is given by

$$\Psi_1 = \{\psi_{11}, \psi_{12}, \psi_{13}, \psi_{14}, \psi_{15}\}$$

where $\psi_{11} = K_p e + kK_p \sum_{i=1}^{n} e_{m,i}$, $\psi_{12} = (1-k)K_p e + kK_p \sum_{i=1}^{n} e_{m,i}$, $\psi_{13} = kK_p \sum_{i=1}^{n} e_{m,i}$, $\psi_{14} = -K'_p e + kK_p \sum_{i=1}^{n} e_{m,i}$, $\psi_{15} = kK_p \sum_{i=1}^{n} e_{m,i} + K_I \int e(t)\,dt$.

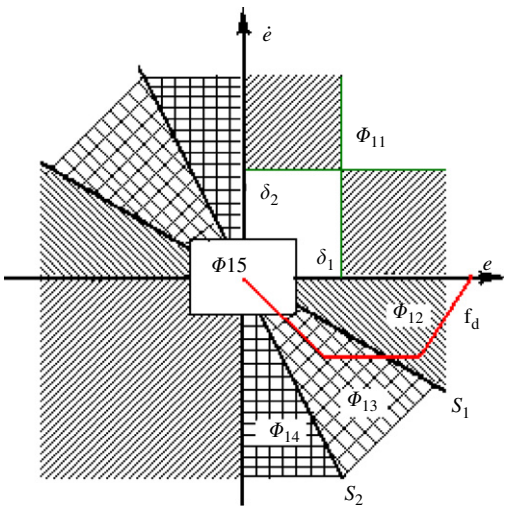

Fig. 6. Characteristic model of direct control level.

In which K_p, k, K'_p, K_I represent proportional coefficient, modified coefficient, modified proportional coefficient and integral coefficient, respectively.

The reference rule set of the direct control level is chosen by

$$\Omega_1 = \{\omega_{11}, \omega_{12}, \omega_{13}, \omega_{14}, \omega_{15}\} \tag{11}$$

where $\omega_{11} \Rightarrow \phi_{11} \rightarrow \psi_{11}$, $\omega_{12} \Rightarrow \phi_{12} \rightarrow \psi_{12}$, $\omega_{13} \Rightarrow \phi_{13} \rightarrow \psi_{13}$, $\omega_{14} \Rightarrow \phi_{14} \rightarrow \psi_{14}$, $\omega_{15} \Rightarrow \phi_{15} \rightarrow \psi_{15}$.

4.2. Parameter correction level

At parameter correction level, the characteristic elements set is chosen by

$$Q_2 = \{q_{21}, q_{22}, q_{23}, q_{24}, q_{25}, q_{26}\} \tag{12}$$

where $q_{21} \Rightarrow |e| < \delta_1$, $q_{22} \Rightarrow |\dot{e}| < \delta_2$, $q_{23} \Rightarrow |e_{m,i}| < \alpha$, $q_{24} \Rightarrow |e_{m,i-1}| < \alpha$, $q_{25} \Rightarrow \Delta e \cdot e \geqslant 0$, $q_{26} \Rightarrow \Delta\dot{e} \cdot \dot{e} \geqslant 0$.

Characteristic model can be written by

$$\Phi_2 = \{\phi_{21}, \phi_{22}, \phi_{23}, \phi_{24}, \phi_{25}\} \tag{13}$$

where $\phi_{21} = \bar{q}_{21} \cap \bar{q}_{22} \cap q_{23} \cap q_{24}$, $\phi_{22} = \bar{q}_{21} \cap \bar{q}_{22} \cap \bar{q}_{23} \cap q_{24}$, $\phi_{23} = q_{21} \cap q_{22} \cap q_{25}$, $\phi_{24} = q_{21} \cap q_{22} \cap \bar{q}_{25} \cap q_{26}$, $\phi_{25} = q_{21} \cap q_{22} \cap \bar{q}_{25} \cap \bar{q}_{26}$.

The reference rule set of the direct control level is shown as

$$\Omega_2 = \{\omega_{21}, \omega_{22}, \omega_{23}, \omega_{24}, \omega_{25}\} \tag{14}$$

where $\omega_{21} \Rightarrow \phi_{21} \rightarrow \psi_{21}$, $\omega_{22} \Rightarrow \phi_{22} \rightarrow \psi_{22}$, $\omega_{23} \Rightarrow \phi_{23} \rightarrow \psi_{23}$, $\omega_{24} \Rightarrow \phi_{24} \rightarrow \psi_{24}$, and $\omega_{25} \Rightarrow \phi_{25} \rightarrow \psi_{25}$.

Parameter correction model set is given by

$$\Psi_2 = \{\psi_{21}, \psi_{22}, \psi_{23}, \psi_{24}\} \tag{15}$$

where $\psi_{21} \Rightarrow K_p = (1 + w_1 e_{m,i}/v)K_p$, $K = 1.1K$, $\psi_{22} \Rightarrow K'_p = (1 - w_1 e_{m,i}/e_{m,i-1})K'_p$, $K = 0.9K$, $\psi_{23} \Rightarrow K_I = w_2$, $\psi_{24} \Rightarrow K_I = -w_2$, and $\psi_{25} \Rightarrow K_I = 0$.

In which w_1 and w_2 denote positive modified coefficients $e_{m,i}$ and $e_{m,i-1}$ represent ith and $(i-1)$th error peak values.

4.3. Task adjustment level

In general, there is no corresponding characteristic model to indicate a task adjustment. All the task adjustments (including the learning process) constitute overall characteristics model of the task adjustment. In this work, task adjustment level deals with the linearization for nonlinear MR damper and control compensation for response time of MR suspension system. A simple feedback control strategy could linearize the response of the MR damper [16]. The control function of damping force can be defined as follows:

$$\begin{cases} F'_d = -c\dot{x} = -c(\dot{x}_s - \dot{x}_u) \\ F_d = F'_d \dfrac{K\chi(I, \dot{x})}{1 + KR\chi(I, \dot{x})} \end{cases} \tag{16}$$

where F_d is the output damping force, F'_d the desired damping force, $\dot{x}$ the damper velocity, I control current, and $\chi(I, \dot{x})$ the quasi-steady damper function with a Bingham plastic. The Bingham plastic model parameters are determined by experimental data fitting. It has been demonstrated that for such a system, by changing the set point gain c and appropriate choices of the forward-loop gain K and feedback-loop gain R, the linear variable damping has been achieved within the control limits. In direct control level, the active damping force F'_d can be gotten; the desired damping coefficient c can be obtained accordingly:

$$c = F'_d/(\dot{x}_s - \dot{x}_u)$$

The forward-loop gain K is modified in parameter correction level according to situation. Feedback-loop gain R is a factor to adjust linear gain in the linearization of MR damper.

The parameters c, K, R, are determined by control algorithms. In other words, the damper is made to operate as a linear "viscous" damper with a damping coefficient that could be directly specified by either the user or by using a hierarchical control strategy. A range of set point gains c, with a linear function, the response (one negative direction) at 1.273 Hz is shown in Fig. 7. It is obvious that there is a good linear relation. The damping force of the MR damper can be fed back with a gain R and compared with the desired force. The feedback scheme in practice will not require a load cell sensor to be placed in series with each MR damper in real time (shown in Fig. 8). The desired damping force is determined by the control algorithms.

Smith [17] proposed a novel method of time-delay compensation, known as Smith's predictor compensation (SPC), by comparing the transfer functions of closed-loop systems with and without time delay. The implementation of the delay compensator $\bar{G}(S)$ requires the delay free gain matrix G, the system model $H(s)$, and the time-delay τ [18]. In the Smith's method, the compensator $\bar{G}(S)$ is designed as follows:

$$\bar{G}(S) = [I + GCH(s)\{I - e^{-s\tau}\}]^{-1} G \tag{17}$$

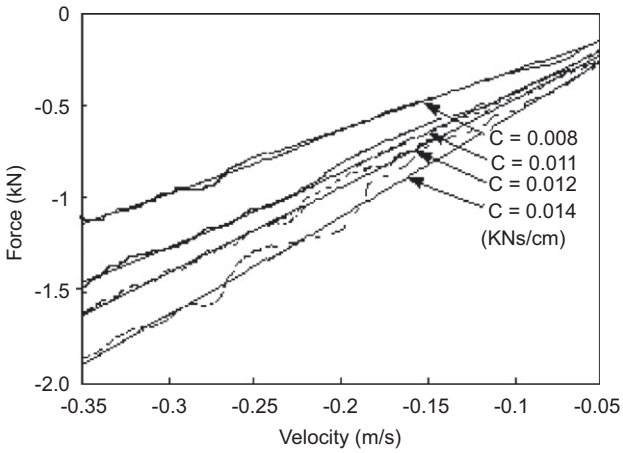

Fig. 7. Simulation result of linearization.

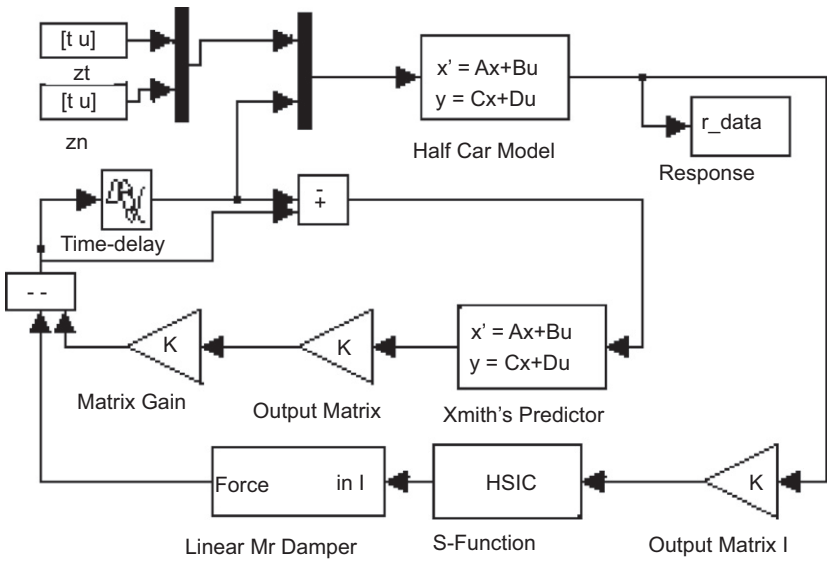

Fig. 8. Block diagram of the semi-active HSIC system.

The Smith's predictor can be implemented in the time domain as the dynamic output compensator [19]:

$$\begin{cases} u(t) = -Gy(t) - Cp(t) \\ \dot{p}(t) = Ap(t) + B\{u(t) - u(t-\tau)\} \end{cases} \tag{18}$$

where $p(t)$ is state variable of Smith's predictor. The implementation of the Smith's predictor can be made through MATLAB SIMULINK block diagram shown in Fig. 8.

The resulting error is scaled using a proportional gain G. It is noted that the proposed semi-active MR damper cannot add energy to the system. When the damping force and the piston velocity have same direction, the HSIC controller can operate. Thus, the damping force can be expressed by

$$F_{\mathrm{MR}} = \begin{cases} F_{\mathrm{MAX}} & \dot{x}_u(\dot{x}_s - \dot{x}_u) \leqslant 0, \quad F'_d > F_{\mathrm{MAX}} \\ -c(\dot{x}_s - \dot{x}_u) & \dot{x}_u(\dot{x}_s - \dot{x}_u) \leqslant 0, \quad F'_d \leqslant F_{\mathrm{MAX}} \\ F_{\mathrm{MIN}} & \dot{x}_u(\dot{x}_s - \dot{x}_u) > 0 \end{cases} \tag{19}$$

5. Control results and discussion

Firstly, the performances of the suspension system under random road excitations are evaluated through computer simulation. The road roughness is Class B represented by a power spectral density function according to ISO 8606 (1995). The vehicle velocity v_0 is 70 km/h, and the delay of excitations between fore wheel and the rear one is given by $\Delta t = l/v_0 = (a+b)/v_0$. The nominal parameters used for the computer simulations are chosen as follows:

$a = 1.3\,\mathrm{m}$, $b = 1.5\,\mathrm{m}$, $m_s = 690\,\mathrm{kg}$, $m_{\mathrm{ur}} = 45\,\mathrm{kg}$, $m_{\mathrm{uf}} = 40\,\mathrm{kg}$, $K_{\mathrm{sf}} = 17{,}000\,\mathrm{N/m}$
$K_{\mathrm{sr}} = 22{,}000\,\mathrm{N/m}$, $k_{\mathrm{tf}} = k_{\mathrm{tr}} = 200{,}000\,\mathrm{N/m}$, $I_y = 1222\,\mathrm{kgm}^2$
$C_{\mathrm{sf}} = 1000\,\mathrm{N/m\,s^{-1}}$, $C_{\mathrm{sr}} = 1100\,\mathrm{N/ms^{-1}}$

In order to demonstrate the effectiveness of the proposed HSIC, conventional LQG control strategy without considering the nonlinearity and time delay of MR suspension is designed and its control performance is compared with the HSIC. The LQG controller is designed on the basis of the following performance index:

$$J = \lim_{T\to\infty} \int_0^T [q_1 \ddot{z}_{\mathrm{sf}}^2 + q_2 \ddot{z}_{\mathrm{sr}}^2 + q_3(z_{\mathrm{uf}} - z_{\mathrm{rf}})^2 + q_4(z_{\mathrm{ur}} - z_{\mathrm{rr}})^2 + q_5(z_{\mathrm{sf}} - z_{\mathrm{uf}})^2 + q_6(z_{\mathrm{sr}} - z_{\mathrm{ur}})^2]\mathrm{d}t \tag{20}$$

In which, $q_1 = q_2 = 1$, $q_3 = q_4 = 1000$, $q_5 = q_6 = 20{,}000$.

Figs. 9 and 10 show the frequency response of acceleration and pitch angle acceleration under random road excitation. The root mean square (rms) comparison of acceleration such as vehicle body acceleration, pitch angle acceleration, and acceleration of the front and rear vehicle axis are shown in Table 3. Using the MR damper controlled by the HSIC controller, the power spectral densities of vertical acceleration and pitch acceleration of the vehicle body are significantly reduced near the body resonance frequency at 1.4 Hz. However, the HSIC gets only limited effort compared with passive suspension at the wheel resonant frequency (10.2 Hz) of the unsprung mass. Between 1.4 and 10.2 Hz, which are the range of human sense, the HSIC can achieve good ride comfort and handle stability. The simulation result indicates that SPC could improve performance of HSIC and HSIC can obtain better effect than LQG.

As a pilot study, four MR dampers are used to replace the passive ones of the test car (Fig. 11a). The HSIC control strategy is downloaded into dSPACE Modular system from Matlab/Simulink. The dSPACE system is fastened in luggage boot and employed to control the four MR dampers, respectively (Fig. 11b). An accelerometer is placed on vehicle body's floor to record the vertical acceleration signal of the sprung mass, and another one is placed on the front axle to record the vertical acceleration signal of the unsprung mass (Fig. 11c and d). A three-dimensional acceleration sensor produced by B&K CO. is placed on driver's seat to calculate weighted root mean square. Every seat has a passenger to hold the vehicle's balance. The test car is

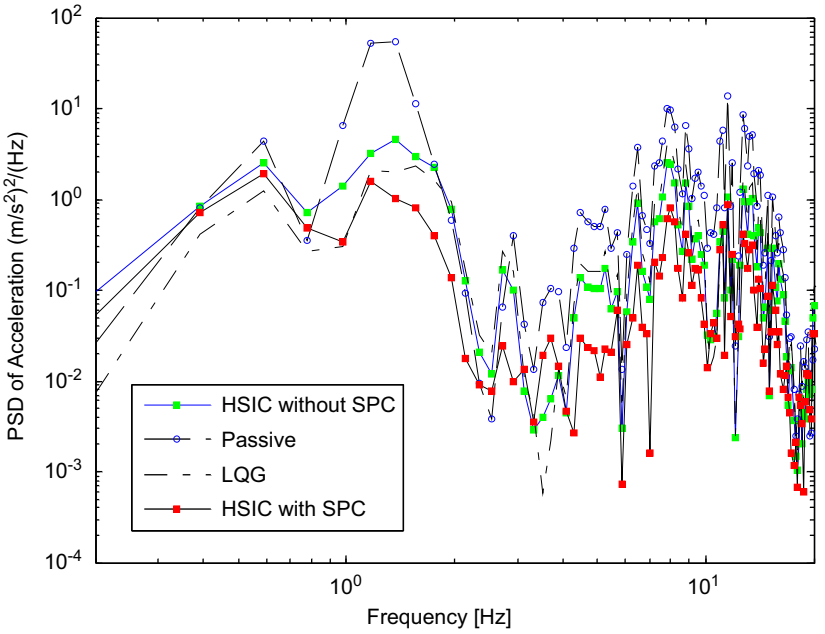

Fig. 9. Power spectral density of body acceleration (simulation).

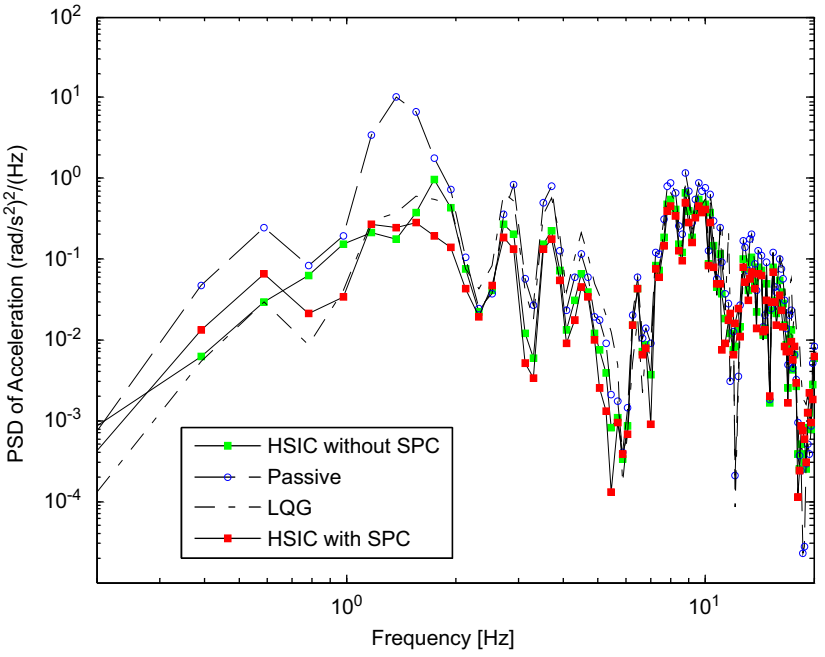

Fig. 10. Power spectral density of pitch angle acceleration (simulation).

driven straight down a concrete road with class B surface (ISO8606, 1995) at 70 km/h (Fig. 12). The cutoff frequency of the lowpass filter is set 50 Hz usually and the sampling frequency is chosen by 200 Hz. Every time the acquired data are divided into 25 sections, each section has 1024 point. Power spectrum density (PSD) of each sampling data is calculated by 1024-point FFT with an average of 25 sections. The results are shown in Figs. 13 and 14. It is clearly observed that the vibration of vehicle body between 1 and 10 Hz is significantly

Table 3
Performance comparison between MR suspension and passive suspension (rms of acceleration by simulation, 70 km/h, road class B)

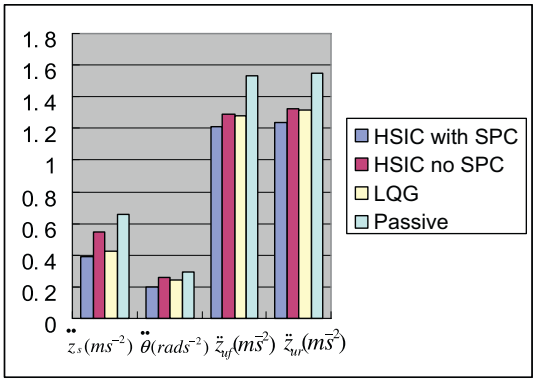

	$\ddot{z}_s$ (m s^{-2})	$\ddot{\theta}$ (rad s^{-2})	$\ddot{z}_{uf}$ (m s^{-2})	$\ddot{z}_{ur}$ (m s^{-2})
HSIC with SPC	0.3856	0.2016	1.2113	1.2402
HSIC no SPC	0.5424	0.2617	1.2861	1.3241
LQG	0.4267	0.2403	1.2814	1.3125
Passive	0.6571	0.2913	1.5353	1.5473

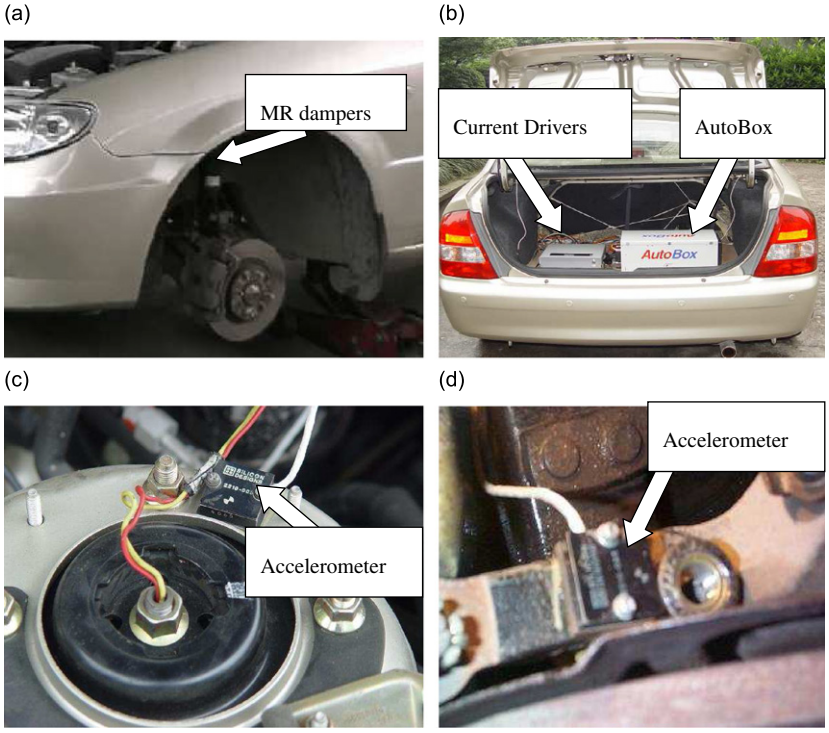

Fig. 11. Setup of the test car. (a) Installation of MR dampers, (b) control systems, (c) sensors installed on sprung mass, (d) sensors installed on unsprung mass.

reduced. However, the semi-active suspension system has minimal effect on suppressing higher mode vibration. LQG has a similar performance to HSIC with SPC in the frequency lower than 1 Hz, but it does not suppress the vibration between 1 and 10 Hz as HSIC with SPC, as we known it is more sensitive by human

Fig. 12. The car test on the road with profile class B.

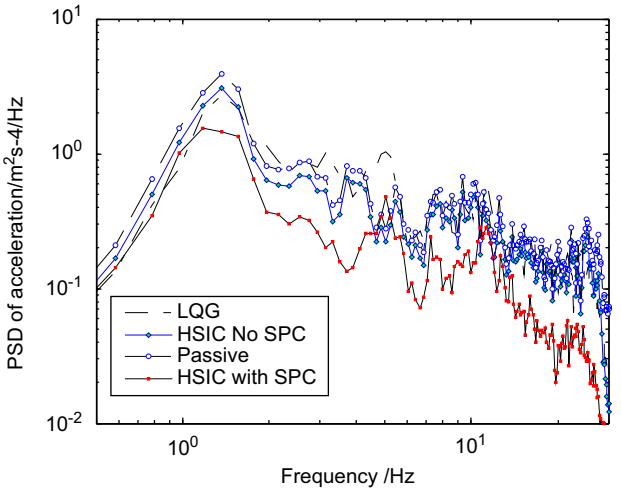

Fig. 13. PSD of body vertical acceleration at 70 km/h (road test).

body. It is obviously that the semi-active suspension with HSIC compared with the passive system can reduce the rms) acceleration of the sprung mass about 27.87% according to Table 4, and SPC can improve the effort of HSIC about 19.9% in rms of acceleration. The vibration of vehicle axes is also depressed as given in Table 4. These results indicate that MR suspension and HSIC controller can improve vehicle's driving security. Some differences exist between test values and simulation results, since the model and parameters of half-car are too rough. But those values have the same regularity, such as the test values also indicates that SPC could improve performance of HSIC and HSIC can obtain better effect than LQG.

On the other hand, it is noteworthy that LQG performs better than HSIC without SPC from the simulated rms results in Table 3 and also test road rms results in Table 4. This is due to the following reasons. HSIC, which has an opening control structure with multi modules, can be developed from modern or classical control theory. Far from excluding LQG, HSIC can embed LQG as its sub-module. Similarly, it can use SPC as a compensation method to improve its control performance. In this study, a specific value τ is chosen as nominal value for HISC to design initial control parameters. Then, according to the changes of system characteristics such as $e_{m,i}$, HSIC will alter control modes or adjust gain parameters to adapt to the fluctuation of τ in the

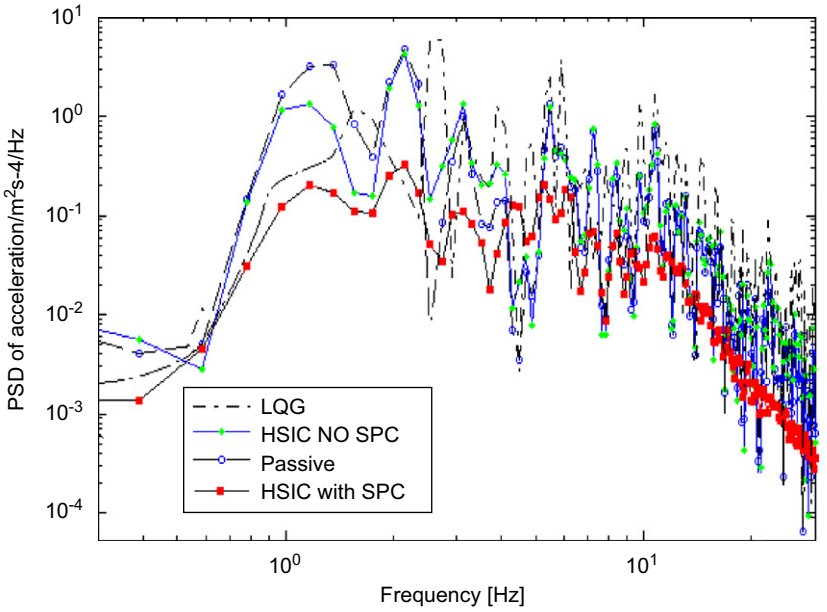

Fig. 14. PSD of body pitch angle acceleration at 70 km/h (road test).

Table 4
Performance contrast of MR suspension and passive suspension (rms of acceleration by Road test, 70 km/h, road class B)

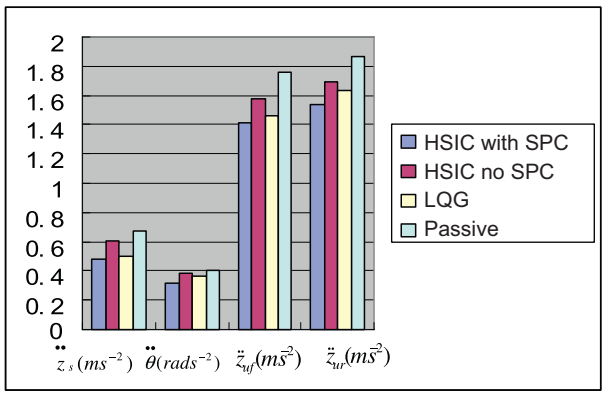

	$\ddot{z}_s$ (m s^{-2})	$\ddot{\theta}$ (rad s^{-2})	$\ddot{z}_{uf}$ (m s^{-2})	$\ddot{z}_{ur}$ (m s^{-2})
HSIC with SPC	0.4826	0.3182	1.4160	1.5343
HSIC no SPC	0.6024	0.3875	1.5769	1.6970
LQG	0.5016	0.3674	1.4632	1.6345
Passive	0.6691	0.4012	1.7643	1.8650

process. The comparison between HSIC without SPC and HSIC with SPC well reflects the advantage of openness of HSIC. In fact, HSIC with or without SPC can all be referred to simply as HSIC. Because the dynamic behavior of MR damper is highly nonlinear, it is difficult to apply a single control method such as LQG to the system directly. Perhaps after optimization of LQG with SPC will provide good performance when τ is a certain value. However, once τ varies, the performance can be unstable. Therefore, a conclusion is made that HSIC can achieve much better performance than LGQ for MR damper applications.

6. Conclusion

In this paper, a controllable semi-active MR damper was devised and applied to vehicle suspension in order to improve ride comfort and handling stability. The time delay of the MR suspension system was experimentally evaluated and integrated with the suspension model. A human simulated intelligent controller was developed to avoid the effect of time delay. Both computer simulation and road test were undertaken in order to demonstrate the effectiveness of the proposed control scheme. Both results indicate that the HSIC can depress automotive vertical vibration and pitch motion. It has been also shown that the Smith predictor compensator could improve performance of the HSIC.

Acknowledgment

This work was supported by the National Natural Science Foundation of China (60404014, 60574074) and the Post-doctoral Fund of People's Republic of China (no. 20070420719).

References

[1] GM Corp. 〈www.chevrolet.com/corvette〉.
[2] J.D. Carlson, D.M. Catanzarite, K.A. St. Clair, Commercial magneto-rheological fluid devices, *Proceedings of the Fifth International Conference on ER Fluids, MR Suspensions and Associated Technology*, Sheffield, UK, 1995, pp. 20–28.
[3] B.F. Spencer, S.J. Dyke, M.K. Sain, J.D. Carlson, Phenomenological model for magnetorheological dampers, *Journal of Engineering Mechanics* 123 (3) (1997) 230–238.
[4] N.M. Wereley, Li Pang, Nondimensional analysis of semi-active electrorheological and magnetorheological dampers using approximate parallel plate models, *Smart Materials and Structures* 7 (5) (1998) 732–743.
[5] U. Dogruer, F. Gordaninejad, C.A. Evrensel, A new magneto-rheological fluid damper for high-mobility multi-purpose wheeled vehicle (HMMWV), in: A. Kon-Well Wang (Ed.), *Proceedings of the SPIE, Smart Structures and Materials 2004: Damping and Isolation*, Vol. 5386, 2004, pp. 195–203.
[6] S.B. Choi, H.S. Lee, Y.P. Park, H_∞ control performance of a full-vehicle suspension featuring magnetorheological dampers, *Vehicle System Dynamics* 38 (5) (2002) 341–360.
[7] Mark O. Bodie, Aleksander Hac, Closed loop yaw control of vehicles using magneto-rheological dampers, *SAE Transactions* 109 (6) (2000) 132–139.
[8] T. Hagiwara, S.A. Panfilov, S.V. Ulyanov, K. Takahashi, O. Diamante, An application of a smart control suspension system for a passenger car based on soft computing, 2003. Available at 〈http://www.yamahamotor.co.jp/global/profile/technical/publish/no35/pdf/0007.pdf〉.
[9] N.K. Petek, D.J. Romstadt, M.B. Lizell, T.R. Weyenberg, Demonstration of an automotive semi-active suspension using electrorheological fluid, SAE Technical Paper Series 950586, 1995.
[10] H. Liu, K. Nonami, T. Hagiwara, Semi-active fuzzy sliding mode control of full vehicle and suspensions, *Journal of Vibration and Control* 11 (8) (2005) 1025–1042.
[11] J. Koo, F.D. Goncalves, M. Ahmadian, An investigation of the response time of magneto-rheological fluid dampers, *Proceedings of the SPIE 2004 Smart Structures and Materials/NDE*, San Diego, CA, 2004.
[12] J.D. Carlson, D.M. Catanzarite, K.A. St. Clair, Commercial magneto-rheological fluid devices, *Proceedings of the Fifth International Conference on ER Fluids*, MR Fluids and Associated Technology, UK, 1995, pp. 20–28.
[13] Zushu Li, Qingchun Chen, Xuemei Li, Hikaru Inooka, Human simulating intelligent control and its application to swinging-up of cart-pendulum, *Proceedings of the Sixth IEEE International Workshop on Robot and Human Communication '97Ro-Man*, Sendai, Japan, 1997, pp. 218–223.
[14] Zushu Li, Hua Zhang, Yongling Wen, GuiPing Wang, Human simulated intelligent control based on sensory-motor intelligent schemas, Intelligent Control and Automation, WCICA 2004, *Fifth World Congress*, Vol. 3, 15–19 June 2004, pp. 2423–2427.
[15] Zhou Qi Jian, Bai Jianguo, An intelligent controller of novel design, *Proceedings of a Multi-national Instrument Conference—part* 1, Shanghai, China, 1983, pp. 137–149.
[16] N.D. Sims, R. Stanway, D.J. Peel, W.A. Bullough, A.R. Johnson, Controllable viscous damping: an experimental study of an electrorheological long-stroke damper under proportional feedback control, *Smart Materials and Structures* 8 (1999) 601–615.
[17] O.J.M. Smith, Close control of loop with dead time, *Chemical Engineering Progress Transactions* 53 (5) (1957) 217–219.
[18] A.K. Agrawal, J.N. Yang, Compensation of time-delay for control of civil, *Earthquake Engineering and Structural Dynamics* 29 (2000) 37–62.
[19] G. Alevisakis, D.E. Seborg, An extension of the smith predictor method to multivariable linear systems containing time-delays, *International Journal of Control* 17 (3) (1973) 541–551.
[20] F. Yu, A. Corolla, An optimal self-tuning controller for an active suspension, *Vehicle System Dynamics* 29 (1998) 51–65.